International Journal of GEOMATE
(Geotechnique, Construction Materials and Environment)
ISSN: 2186-2982 (P), 2186-2990 (O), Japan
Vol. 31, Issue 144, August, 2026, PP.1-19; DOI: 10.21660/2026.144.5630

# A SYSTEMATIC REVIEW OF GEOGRID-REINFORCED SOIL RETAINING WALL: ANALYSIS METHODS AND DETERMINATION OF CRITICAL DESIGN PARAMETERS

*Yujia Wang[1]

[1]School of Civil Engineering, Southwest Forestry University, Kunming, China

*Corresponding Author, Received: 27 April 2026, Revised: 18 May 2026, Accepted: 26 May 2026

**ABSTRACT:** The geogrid-reinforced soil retaining wall plays an important role in the stabilization of both natural and engineered soil slopes, and the effectiveness of this kind of slope stabilization method has been proven by extensive engineering practice. A wide variety of literatures have conducted research on the behavior and performance of geogrid-reinforced soil retaining walls by various methods, however, it still remains a significant challenge to figure out this specific reinforcement mechanism that involves the interaction between the soil and the geogrid layers. Numerous numerical methods and analytical methods have been derived and purposed to study the mechanism of geogrid reinforcement, as well as the behavior of slope and the performance of geogrid layers subject to various conditions. To provide a solid foundation for the understanding of geogrid reinforcement mechanism, the internal, external, and overall instability mode of geogrid-reinforced soil retaining wall has been compared and discussed. The design methods of geogrid-reinforced soil retaining wall include Earth Pressure Theory, Limit Equilibrium Method, and Finite Element Method have been summarized and discussed with respect to their basic concepts and utilizations. The effect of critical design parameters of geogrid-reinforced soil retaining wall including wall-facing inclination, the reinforcement length, and the reinforcement spacing are important for the understanding of the behavior of geogrid-reinforced soil retaining wall, which therefore have been discussed and reviewed thoroughly from the literature.

*Keywords: Slope stability, Geogrid-reinforced soil retaining wall, Analysis method, Critical design parameters*

## 1. INTRODUCTION

The geogrid-reinforced soil retaining wall (GRS-RW) has been extensively utilized as an effective method in many regions since its first introduction in 1970 because of the increasing infrastructural development demands, especially for road embankments and slopes in urban regions. The benefits of using GRS-RW for the stabilization of slopes and road embankments include the expediency of construction, outstanding seismic performance, cost-effectiveness, ability to tolerate large differential settlements, and the aesthetic appeal [1]. The effectiveness of GRS-RW on improving the stability of slopes has also been comprehensively demonstrated [2-9]. In these applications the role of geogrid layers is to provide resistance to the sliding forces or moments induced by self-weight of the structure or the surcharge load applied on the structure. Together with the wall-facing ranges from the rigid concrete panels to the more flexible units such as the steel mesh or the gabion basket, the backfill of the wall can be retained firmly and the soil surface erosion can be prevented effectively. As a preventive measure to stabilize active landslides, a wide variety of analysis methods have been developed and proposed to investigate the behavior and performance of GRS-RW [10-14]. The existing analysis methods for GRS-RW can be categorized into three main types: (1) Earth Pressure Theory [10, 11]; (2) Limit Equilibrium Method [12, 15, 16]; (3) Finite Element Method [13, 17-19]. Regarding Earth Pressure Theory for the design of GRS-RW, it is assumed that the tensile forces within the geogrid layers are in equilibrium with lateral earth pressure in mechanically stabilized earth walls. With respect to Limit Equilibrium Method, it has been adopted extensively in the analysis of slope stability. The most commonly used techniques of Limit Equilibrium Method are methods of vertical slices, including the ordinary method of slices, the Bishop simplified method, Janbu, Morgenstern-Price, and Spencer methods [20-23]. Moreover, the Limit Equilibrium method has also been extended to the design of GRS-RW by incorporating the stabilization effect contributed from the geogrid tensions into equilibrium analysis (balance of the moment or inter-slide force) under the critical limit state. For Finite Element Method, it has been proved as an effective method in studying the complicated behaviors of the reinforced soil structures, and also a supplement to the conventional Limit Equilibrium Method. The boundary conditions and the interface behavior between the geogrid layers and the soils can be considered adequately, and a wide variety of loading conditions can be applied to the numerical model, i.e., static loading conditions, dynamic loading conditions such as the traffic and seismic loading conditions, and the staged loading conditions to represent the construction process.

Compared with other types of conventional retaining structures, the GRS-RW has its own advantages for the stabilization of slopes and road embankments. Due to these economical and technical advantages and the growing demands in the construction of GRS-RW for infrastructural developments, it is therefore important to understand the performance and the behavior of the GRS-RW related to critical design parameters including the wall-facing inclination, the reinforcement length, and the vertical spacing between layers of the reinforcement. These parameters have considerable impacts on the location and shape of the potential critical slip surface, the horizontal displacements and vertical settlements, and the tensile loads and strains within the reinforcement [19]. Moreover, these critical design parameters of GRS-RW would impose impacts on the engineering cost as well as the failure mode, therefore, a thorough review on these critical design parameters would be a useful reference for the design of GRS-RW to keep a balance between the engineering cost and performance.

As a well-developed slope-stabilization method, a wide variety of research has been conducted on GRS-RW to study its reinforcing mechanism, geogrid-soil interactions, failure mode as well as the deformation pattern. Therefore, in this study, the methods for the analysis of GRS-RW are summarized and reviewed firstly, with a focus on the Finite Element Method. In addition, the effect of critical design parameters on performance of GRS-RW is also compared and discussed. In the present study, a systematic review of the GRS-RW is carried out, and these discussions and summarizations would deepen the understanding of the GRS-RW that has been used extensively for the stabilization of slopes. Moreover, the current study also provides valuable theoretical references and technical guides for the optimal design, performance improvement, and innovative application of this type of retaining structure for future engineering practices.

## 2. RESEARCH SIGNIFICANCE

The geogrid-reinforced soil retaining wall plays a significant role in the stabilization of the embankment and the slope, the current study comprehensively reviews the typical failure mode, analysis methodology, and the effects of critical design parameters. The review, discussion, and summarization of characteristics of geogrid-reinforced soil retaining wall in this study can provide a scientific basis for engineering design and lays a foundation for subsequent studies on geogrid-soil interaction and seismic performance, which holds a significant engineering practical and academic value.

## 3. TYPICAL FAILURE MODES OF GRS-RW

### 3.1 External Instability

Regarding the external stability evaluation of GRS-RW, the geogrid-reinforced soil section is treated as a homogeneous composite soil mass, and the stability of the retaining structure is assessed based on the failure modes for conventional gravity retaining wall type. The typical external failure modes of the GRS-RW are illustrated in Fig. 1. The failure mechanisms of the external instability can be used to determine the dimensional parameters of the geogrid-reinforced soil section including the wall-facing to guarantee this homogeneous composite soil mass has sufficient size against the sliding, overturning at the toe, bearing capacity failure of the foundation soil, as well as the deep-seated instability.

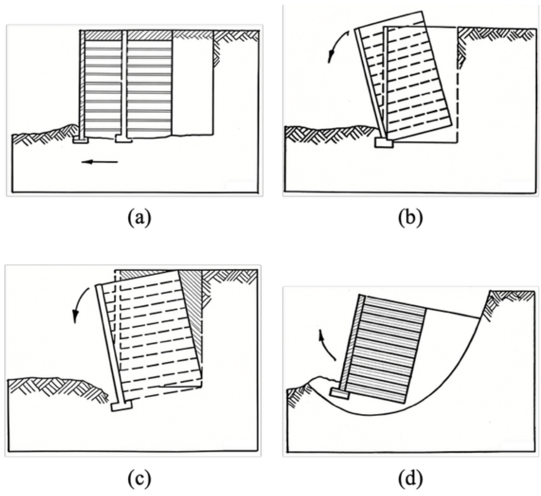


Fig. 1. Typical external failure mechanisms for GRS-RW: (a) sliding; (b) overturning; (c) bearing capacity failure; (d) deep-seated instability [10]

### 3.2 Internal Instability

With respect to the internal stability evaluations, the component involved in the geogrid-reinforced soil mass is treated separately. This principle indicates that the deformations of the retaining wall are restricted by the geogrid reinforcement rather than the homogeneous composite soil mass. The internal failure mode can be used to analyze the effect of the reinforcement length, spacings, and the properties on the behavior of the retaining structure. In other words, the vertical spacing between layers of geogrid reinforcement, the length and the tensile strength of the geogrid will affect the pattern of the internal failure. In addition, the internal failure mode of the GRS-RW can be categorized into two types (Fig. 2): (1) The tensile forces within the reinforcement become relatively large and then the reinforcement excessively elongates or breaks, leads to the large displacement or the possible failure of the retaining structure. This internal failure mode is tensile over-stress (Fig. 2a); (2) When the tensile forces within reinforcements are larger than the pullout resistance of the structure, i.e., the force can pull the reinforcements out of the reinforced soil mass, the shear stresses of the surrounding soil will increase significantly and the large displacements or the structure collapse may occur. This kind of internal failure mode can be regarded as the failure by pullout (Fig. 2b).

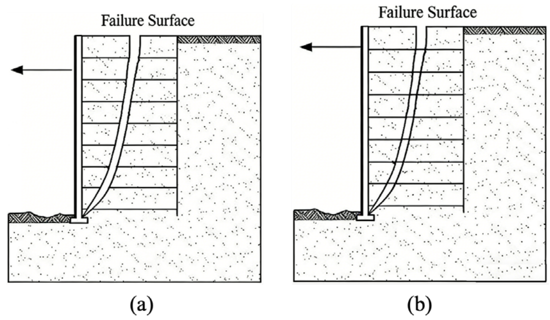


Fig. 2. Typical internal failure mode of GRS-RW: (a) tensile over-stress failure; (b) pullout failure [24]

### 3.3 Overall Instability

For the overall instability mode, when the GRS-RW is constructed on the slope, the stress field within the slope mass will be altered significantly and the slope failure away from the retaining structure vicinity may be triggered. This failure pattern mainly depends on the geometry of the slope and the properties of the soil and the geogrid reinforcement. The methods adopted to evaluate the overall instability conditions can be derived from the method for the analysis of slope stability. The modified Bishop's method can be used when the circular failure surfaces can be assumed, and this conventional method can yield satisfactory results. The overall instability of the reinforced structure constructed on the slope can be depicted in Fig. 3.

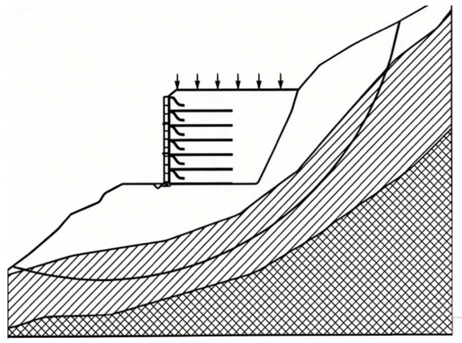

Fig. 3. Overall instability condition of GRS-RW [25]

## 4. ANALYSIS METHODS FOR GRS-RW

### 4.1 Earth Pressure Theory

Regarding the design guidelines for GRS-RW, the Earth Pressure Theory that has been utilized extensively to evaluate the tensile forces within the geogrid reinforcement. It is assumed that the tensile forces within the geogrid reinforcements are in the equilibrium with the lateral earth pressure in GRS-RW. To predict the maximum tensile forces generated within each layer of the geogrid reinforcement, the first step is to calculate the active earth pressure coefficient based on the Coulomb earth pressure relationship. For GRS-RW with vertical wall-facing, the earth pressure can be reduced to Rankine's equation:

$$K_a = \tan^2(45 - \varphi'/2) \tag{1}$$

where $K_a$ is the coefficient of active earth pressure. Regarding the inclinations of the wall-facing equal or greater than $8^{\circ}$ from the vertical, the Coulomb equation in the following simplified form can be utilized:

$$K_a = \frac{\sin^2(\theta+\varphi')}{\sin^3\theta(1+\frac{\sin\varphi'}{\sin\theta})^2} \tag{2}$$

where $\theta$ is the inclination of the wall-facing as measured from the horizontal starting in front of the wall. Then, the maximum tensile forces within each geogrid reinforcement layer can be given by:

$$T_{max} = \left(\frac{k_r}{K_a}\right) K_a \gamma z S_V \tag{3}$$

where $T_{max}$ represents the maximum tensile force of per unit width geogrid reinforcement; $k_r/K_a$ denotes the normalized coefficient of horizontal earth pressure (Fig. 4); $K_a$ is Rankine active earth pressure coefficient; $\gamma$ represents the unit weight of the backfill; $z$ denotes the depth of the reinforcement below the top of the reinforced wall; $S_V$ is the vertical spacing between the geogrid layers.

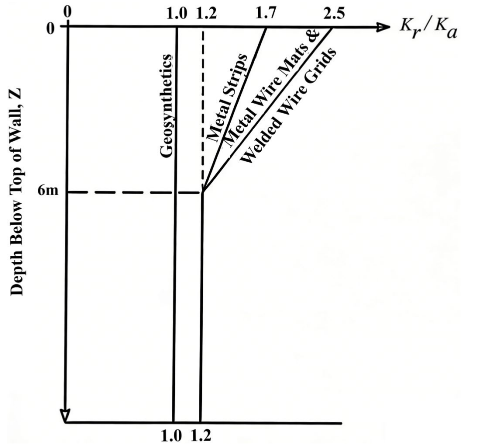


Fig. 4. Stress ratio for various reinforcement with depth in GRS-RW [10]

The normalized stress ratio $(\boldsymbol{k_r/K_a})$ for various types of geogrid reinforcement along the depth of the GRS-RW is depicted in Fig. 4. The value of stress ratio $(\boldsymbol{k_r/K_a})$ for the GRS-RW is constant throughout the depth of the wall and remains at $\mathbf{1.0}$. This phenomenon represents that for the GRS-RW with the extensible reinforcement such as the geogrid, the soil can reach active stress state and generate sufficient active earth pressure induced by the horizontal displacement during the construction process. Regarding the GRS-RW with stiff reinforcement such as metal strip, the movement of the soil especially near the top of the wall is restricted, which represents that the full strength of the soil is not mobilized sufficiently, the reinforcement near the top of the wall thus resists a higher lateral earth pressure. According to Fig. 4, the value of the normalized stress ratio $(\boldsymbol{k_r/K_a})$ for the steel reinforcement is higher at the top of the wall ranges from $\mathbf{1.7}$ to $\mathbf{2.5}$, and then decreases to $\mathbf{1.2}$ at the depth of $\boldsymbol{6\ m}$.

After the calculation of the maximum tensile forces $(T_{max})$ within the geogrid reinforcement layer, internal stability of GRS-RW respect to pullout failure of the geogrid reinforcement can be checked by:

$$T_{max} \leq \frac{1}{FS_{PO}} F^* \gamma Z_p L_e C R_C \alpha \tag{4}$$

where $FS_{PO}$ is the Factor of Safety with respect to pullout failure which $\geq 1.5$; $T_{max}$ denotes the maximum tensile forces within the reinforcement; $C$ is 2 for reinforcement types of sheets, strip, and grid; $\alpha$ represents the factor for scale correction; $F^*$ denotes the resistance factor for pullout failure; $R_c$ is the coverage ratio; $\gamma Z_p$ represents the overburden pressure includes the distributed static surcharge loads; $L_e$ denotes the embedded length of the reinforcement in the resisting zone. Consequently, the minimum embedded length of the geogrid reinforcement in the resisting zone which beyond the potential failure surface can be given by:

$$L_e \geq \frac{1.5 T_{max}}{C F^* \gamma Z_p R_C \alpha} \geq 1\ m \tag{5}$$

Each layer of the reinforcement should satisfy the criterion, otherwise the length of the geogrid reinforcement needs to be increased, and/or the geogrid reinforcement with a larger tensile strength needs to be used, and the vertical spacing between layers of the geogrid reinforcement may be decreased.

Each analytical method has limitations, and the limitations of the design method based on the Earth Pressure Theory have been summarized as follows: (1) This lateral earth pressure-based approach may be overly conservative for the GRS-RW; (2) Difficult to apply to the case with complicated geometry, such as the multi-tiered walls and narrow walls; (3) This approach is only limited to uniform granular soil and is relatively difficult to apply to non-ideal filling; (4) The pore-water pressure within the reinforced filling is neglected; (5) The global stability of GRS-RW is not determined; (6) The deformation of GRS-RW or the filling soil is not evaluated [11]. In general, the lateral earth pressure-based Earth Pressure Theory design method for GRS-RW can guarantee the safety of the retaining structure, but may be overly conservative with respect to the evaluation of the geogrid reinforcement strength for GRS-RW on relatively firm foundations and the neglection of pore-water pressure within the reinforced filling soil. The seepage force within the structure is not considered and sufficient drainage is assumed in this method.

### 4.2 Limit Equilibrium Method (LEM)

The Limit Equilibrium Method (LEM) has been extensively adopted in the analysis of slope stability. A comprehensive review of commonly used limit equilibrium techniques for the evaluation of slope stability has been conducted [26]. Moreover, the LEM has also been extended to the design of GRS-RW. The stabilization effect contributed from the geogrid reinforcement tensions is incorporated into the equilibrium analysis under the critical limit state. As two types of the material, the geogrid reinforcement and the soil filling, involved in the retaining structure, the analysis is relatively more complex: a wider variety of failure mechanisms exists in the retaining structure, and the slope stability analysis thus requires more assumptions. For different limit equilibrium-based analytical methods, the assumption of the inclination of the force between vertical slices of reinforced soil mass is various. Compared with traditional limit equilibrium analysis, additional major assumptions including the peak tensile forces within each layer of the reinforcement and the distribution of the reinforcement tension along with the depth are required.

The analytical method using LEM can be categorized into two main types. The first category uses the simple analysis of the force equilibrium which represents that the horizontal forces from the soil mass are balanced by the total reinforcement forces to avoid the instability of the slope [15, 27-30]. The second category of the method evaluates the equilibrium state of the force and/or the moment on the pre-assumed critical failure surface with the consideration of the balancing moment and force contributed by the reinforcement layers [16, 31]. These design approaches for GRS-RW provide a unified method for the analysis of the retaining structures and slopes, i.e., the contribution from facing blocks of GRS-RW to the stability of the slopes has been considered, and the additional effect from the friction between the facing blocks of GRS-RW was also involved in the design method of the reinforced retaining structure [16, 32].

As a simple method for the design of GRS-RW, the method which assumes a circular arc slip surface and satisfies the vertical force equilibrium and the moment equilibrium of a given body, has been widely used in routine practice [20]. The soil mass is defined by a circular arc slip surface and the soil surface is divided into $\boldsymbol{n}$ vertical slices (Fig. 5). It is notable that the surcharge load applied on slice $\boldsymbol{i}$ is represented by the vertical forces ($\boldsymbol{Q_{vi}}$) and the horizontal forces ($\boldsymbol{Q_{hi}}$), and the reinforcement layer also horizontally intersects the base of slice $\boldsymbol{i}$. Extracting slice $\boldsymbol{i}$ from the soil mass, the forces acting on the free body of slice $\boldsymbol{i}$ can be obtained (Fig. 6). The other forces acting on the slice such as the force induced by the pore-water force is not shown for clarity. These forces acting on the body of slice $\boldsymbol{i}$ (with the seismic forces or reinforcement forces) are considered when satisfying the global moment equilibrium and the vertical force equilibrium. After the inclusion of the geogrid reinforcement as a known force, the Safety Factor (SF) associated with a soil mass defined by a circular slip surface with a radius $\boldsymbol{R}$, can be given by:

$$\boldsymbol{SF} = \frac{\sum\left\{\frac{[c'_i \Delta x_i + (W_i + Q_{vi} - u_i \Delta x_i)] \tan\varphi'_i}{m_{\alpha i}}\right\}}{\sum\left[(W_i + Q_{vi}) \sin\alpha_i + \frac{Q_{hi} d_i}{R} - T_i R_c \cos\alpha_i\right]} \quad (6)$$

and supplemented with

$$m_{\alpha i} = \cos\alpha_i + (\sin\alpha_i \tan\varphi'_i)/SF \quad (7)$$

where $\boldsymbol{c'_i}$ and $\boldsymbol{\varphi'_i}$ are the effective cohesion and the effective friction angle of the soil at the base of slice $\boldsymbol{i}$, $\boldsymbol{u_i}$ denotes the average pore-water pressure acting on slice $\boldsymbol{i}$ base, $\Delta \boldsymbol{x_i}$ represents the width of slice $\boldsymbol{i}$, $\boldsymbol{d_i}$ is the vertical distance from the component of the horizontal force of the surface surcharge load to the center of the analyzed circular failure surface, $\boldsymbol{R_c}$ represents the reinforcement coverage ratio, and $\boldsymbol{T_i}$ denotes the horizontal reinforcement force acting at the base of the slice $\boldsymbol{i}$.

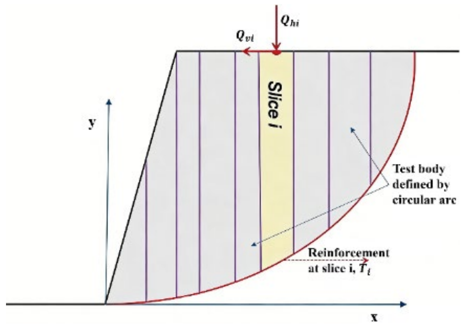


Fig. 5. Circular soil mass defined in the Bishop method [12]

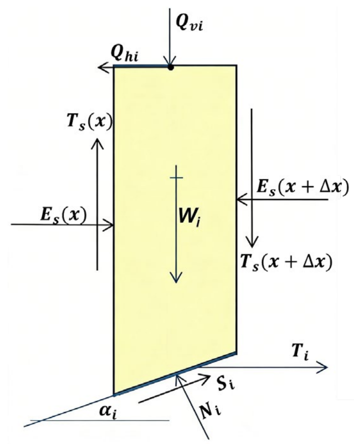


Fig. 6. Forces applying on the slice $\boldsymbol{i}$ [12]

Compared with Earth Pressure Theory-based design methods for GRS-RW, LEM has the following advantages: (1) LEM can be used for the design of slope cases with complex geometry, i.e., the narrow-reinforced walls or multi-tiered reinforced walls; (2) The effect of the pore-water pressure on the stability of the reinforced wall can be considered; (3) The global stability of the GRS-RW as well as the local stability at any prescribed failure surface can be evaluated; (4) LEM is a numerically stable method that can yield close results with respect to Factor of Safety (FoS) and the slip surface location to complex rigorous methods such as Finite Element Method [33, 34]. Moreover, the limitations of the design method based on LEM have been summarized as follows: (1) The effect of the connection load on the stability is not considered within the framework of the LEM; (2) The distribution of the geogrid reinforcement tensile forces is assumed as a uniform pattern in which the peak reinforcement tensions are proportional to the overburden pressure, this assumption needs additional verification; (3) The effect of the downdrag at the connections is not considered; (4) The deformation of the GRS-RW and the soil mass is not considered [11]. In general, appropriate utilization of LEM can address various issues of the GRS-RW design when adopting different failure mechanisms. With the development in the LEM, the GRS-RW can be designed economically and effectively in this framework.

### 4.3 Finite Element Method (FEM)

Numerical modelling, including the Finite Element Method (FEM), has become an effective method in studying the complex behavior of the GRS-RW, and also a supplement to the conventional LEM. FEM has been extensively applied to simulate the behavior of the GRS-RW under various working scenarios [13, 18, 35-37]. Overall, compared with the analytical methods, the advantages of the FEM are considered as follows: (1) The full continuum mechanics are considered in FEM, i.e., the constitutive relationship of all materials are adopted in the analysis; (2) The boundary conditions and the interface behavior between the geogrid reinforcements and the soil are considered adequately, and a wide variety of the loading conditions can be applied to the numerical model, i.e., static loading conditions, dynamic loading conditions such as the traffic and seismic loading conditions, and the staged loading conditions to represent the construction process; (3) The compatibility of the displacements between various materials is guaranteed; (4) FEM can provide a general view of the distribution of the displacement, force, stress and strain within the geogrid reinforced soil mass.

A previous study carried out a finite element analysis on the behavior of the GRS-RW with a height of $\mathbf{8}\,\boldsymbol{m}$ constructed on a layered foundation [17]. The layer-by-layer construction sequence of the wall was considered, while the compaction stress that occurred during the construction process was ignored. The numerical results obtained from the finite element analysis were then compared with the measurements from a full-scale test wall. The result indicates that the strength and stiffness of the foundation soil significantly affect the behavior of the GRS-RW, especially for the GRS-RW constructed on the weak foundation. Compared with the performance of the GRS-RW constructed on the rigid foundation, the high compressible and weak foundation significantly increases the wall-facing displacement and the strain magnitude within the geogrid reinforcement layers. For the horizontal stress behind the wall-facing, its distribution is not significantly influenced by the types of foundation that vary in strength or stiffness. Another study conducted a finite element numerical analysis on a $\mathbf{6}\,\boldsymbol{m}$ high GRS-RW constructed on a $\mathbf{10}\,\boldsymbol{m}$ yielding foundation under bridge abutment loads and road loads [38] (Fig. 7). It is notable that surcharge loads from bridge abutment and traffic result in a normally consolidated yielding in the foundation and the failure mainly happens in the foundation layer below the reinforced soil zone. It has also been found that the GRS-RW can tolerate excessive displacements and reduce differential settlements at the surface of backfill caused by the yielding in the foundation layer. Moreover, for the GRS-RW that has sufficient safety margin, the effect of increasing stiffness and length of bottom layer of geogrid reinforcement on the global stability is limited. The researchers carried out a numerical analysis on the construction of four full-scale reinforced retaining walls and their response subjected to uniform surcharge loading [39] (Fig. 8). The effect of compaction on sand backfills and the type of geogrid reinforcement on behavior of GRS-RW under uniform surcharge loading conditions has been investigated. The result from the numerical analysis indicates that the elastic modulus of the soil needs to be modified to accommodate the compaction effect during the construction of GRS-RW. In addition, the assumption of a perfect bond between the sand backfills and the reinforcement layers may not be appropriate and the slippage between the soil and the geogrid reinforcement layers should be considered for further studies.

To study the response of GRS-RW subjected to the wide range of surcharge load levels, another study carried out full-scale load tests and three-dimensional finite element analysis on a $\mathbf{5}\,\boldsymbol{m}$ height GRS-RW [40]. The performance of GRS-RW subjected to the surcharge load under the working conditions was evaluated and then complete set of data was used for the validation of three-dimensional finite element analysis.

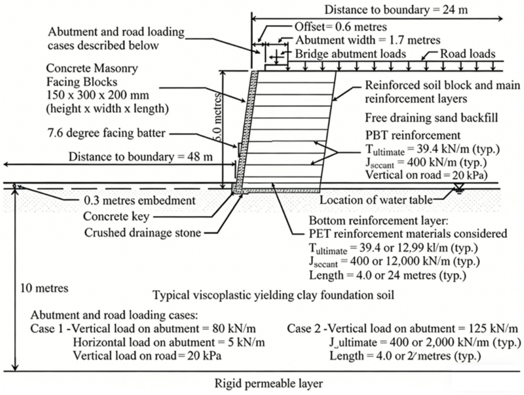


Fig. 7. Cross-section of GRS-RW under surcharge load of bridge abutment and traffic [38]

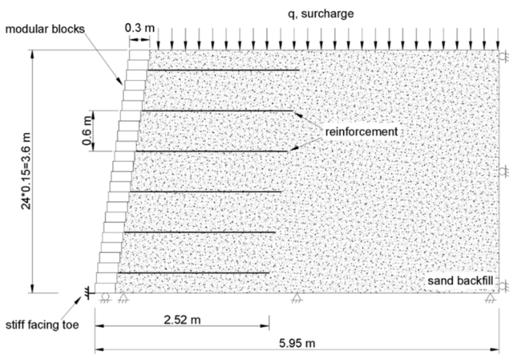


Fig. 8. The geometry of tested reinforced wall [39]

The results from the load test indicated that the maximum wall-facing displacement and the maximum strains within the geogrid reinforcement layer under the working level surcharge load were relatively small, and a good load carrying capacity of GRS-RW thus can be demonstrated (Fig. 9). In the three-dimensional finite element analysis that adopted the higher value of the surcharge load, the results indicated that the load carrying capacity of GRS-RW is governed by the backfill soil bearing capacity failure rather than the failure of the geogrid reinforcement layers. A previous study conducted a numerical study to investigate the effect of the soil constitutive model on the prediction of the behavior of two full-scale GRS-RW at the end of construction and under surcharge loading conditions [41]. The result from numerical analysis indicates that there are detectable differences among the response of GRS-RW simulated with three different constitutive models under various surcharge loading conditions, while the predictions are still within the range of the measured values. In general, the appropriate modelling of the interface behavior and the nonlinear behavior of geogrid reinforcement layers is as important as the determination of the soil constitutive model for an accurate simulation. Another study carried out a numerical analysis on the effect of backfill soil, reinforcement types, and soil-geogrid interface on the behavior of GRS-RW under the serviceability limit state (SLS) and the ultimate limit state (ULS) [42] (Fig. 10). They found that the geogrid reinforcement yields larger horizontal wall-facing displacements than the metallic reinforcement. The soil shear strength was found to affect the deformation and the stability of the GRS-RW to a larger extent. The shear stiffness of the interface between the geogrid reinforcement layer and the backfill soil governs the deformation of the wall-facing to a large extent, thus a reasonable estimation of this parameter is required for the evaluation of GRS-RW displacements.

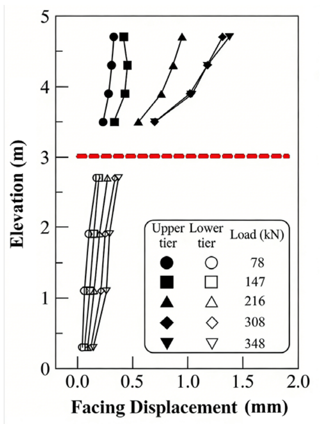


Fig. 9. Facing displacement profiles at various loading stages [40]

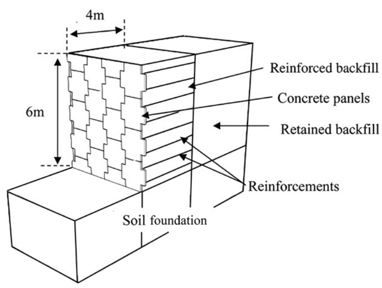


Fig. 10. Geometry of the numerical model [42]

The researchers conducted a numerical parametric study of the geogrid reinforced slope by changing the parameters including the geogrid layer placement depth, number of layers, vertical spacing between geogrid layers, Young's modulus, thickness, and the embedded length of the geogrid [43]. By redistributing the loads and restricting the development of the failure surface, the geogrid reinforcements were found to be advantageous in restraining the displacements of slopes and improving the stability of the slope. The geogrid reinforcement placement depth also governs the location of the maximum horizontal displacement and the stability of the reinforced slopes to a large extent (Fig. 11). The compaction in the backfill soil leads to the increase in the vertical stress and the shearing resistance of the interface between the soil and the reinforcement, therefore, the maximum tensile stress mobilized within the geogrid reinforcement layer also increases significantly. They also found that the optimal location of the geogrid reinforcement placement is between the middle of the critical slip surface of the unreinforced slope and the middle of the slope. Another study conducted a numerical analysis to investigate the load transfer mechanisms within GRS-RW which comprise of the steel strip reinforcement and the concrete wall-facing panel utilizing the FEM (PLAXIS) and the Finite Difference Method (FDM) (FLAC) [44]. It has been found that increasing the modulus of the backfill soil leads to a decrease in the tensile loads within the geogrid reinforcement layer. With the increase in the modulus of the backfill soil and surcharge loads, the difference in the predicted reinforcement tensile stress between PLAXIS and FLAC appears. Moreover, the increase in the tensile loads of the geogrid reinforcement induced by the increase in the interface stiffness predicted in two programs shows a good consistency. The development of detailed numerical models utilized to predict the behavior of the wrapped wall-facing GRS-RW with the height of $\mathbf{3.6\,m}$ has been described by [45]. The numerical results of the wall behavior in terms of the reinforcement loads and strains, foundation pressures, and the wall-facing displacements are then compared with the measured values. The difference of the wall-facing displacement profile was observed between the numerical prediction and the measured values, and the numerically predicted tensile loads and the strains within the reinforcement layer were larger than the measured values (Fig. 12). The poor agreement in the wall-facing displacement profile between the numerical results and the measured values can be attributed to the excessive flexibility of the wrapped wall-facing which cannot be accurately simulated. In addition, the unquantifiable factors such as the quality of the material and the construction techniques also impose impacts on the wrapped wall-facing movements during construction. Moreover, a previous study carried out a numerical analysis of the combined effect of the wall facing inclination, compaction-induction stress, wall height, and the width of the surcharge load on the behavior of the GRS-RW [19]. $\mathbf{21}$ numerical simulations have been resulted from the variation in 4 aforementioned factors for the parametric study including wall-facing inclination ($\mathbf{1:10}$, $\mathbf{1:6}$, and $\mathbf{1:3}$), compaction-induced stress (without compaction, $\mathbf{60\,kPa}$, and $\mathbf{120\,kPa}$), wall height ($\mathbf{3.6\,m}$, $\mathbf{6.2\,m}$, and $\mathbf{12.4\,m}$), and surcharge load width ($\mathbf{0.6\,m}$, $\mathbf{1.2\,m}$). The result from the numerical analysis indicates that there is a threshold value of the surcharge load width beyond which the tensile loads within the reinforcement layer will not be influenced further, while the horizontal wall-facing displacement can still be affected by the increase in the surcharge load width. The compaction on the backfill surface during the construction was found to induce the soil mass movements and increase the tensile loads within the reinforcement layer, which can be regarded as a type of the prestress within the reinforced soil zone and the post construction movements of the soil mass can be effectively reduced by this effect.

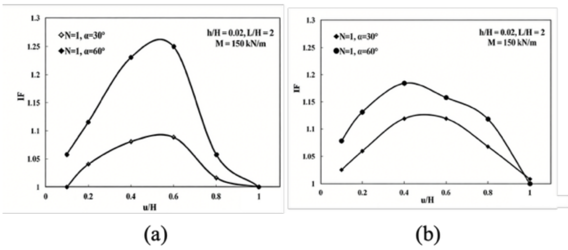


Fig. 11. Effect of depth of geogrid placement: (a) sandy soil; (b) clayey soil [43]

Although the finite element analysis has been extensively used as it can provide reasonable predictions on the performance of the GRS-RW with a wide range of information, the limitations of the finite element analysis has been discussed as follows: (1) a comprehensive characterization of the strength properties of the wall-facing, the reinforcement layers, and the backfill soil and the foundation soil is required for a reasonable numerical predication of the GRS-RW behavior; (2) it requires intensive computational effect, and the development in the computer program has significantly simplified the computational cost; (3) it requires careful modelling and adjustment to consider the effect of the interface behavior between the reinforcement and the soil reasonably; (4) the numerical predictions on the GRS-RW wall behavior may be non-conservative, reliable input parameters and appropriate safety and/or resistance factors are required for the reasonable evaluation of the wall behavior [11].

Moreover, for the issue of the large strain or the deformation of the GRS-RW, the finite element analysis may yield unreasonable predictions on the wall behavior. For flexible structures such as GRS-RW, the issue of the large deformation is critical for an accurate assessment on the performance of the structure.

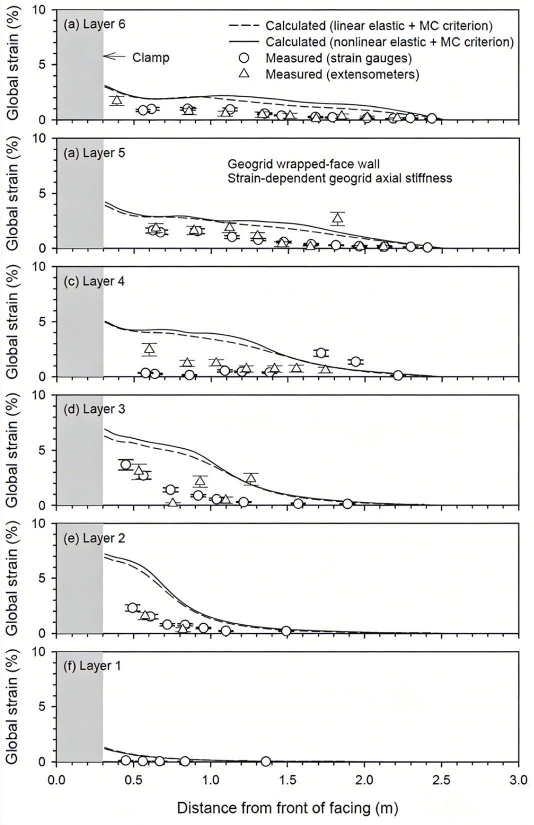


Fig. 12. Measured and calculated reinforcement strains [45]

Therefore, some specific implementations and developments in finite element analysis are required for the simulation of GRS-RW under large deformation conditions, such as a more advanced constitutive model of the soil that can represent the post-peak behavior of the soil. In addition, special care is also needed for the occurrence of the numerical instability during the simulation of GRS-RW behavior under the large strain/deformation conditions.

## 5. DETERMINATION OF CRITICAL DESIGN PARAMETERS

### 5.1 Effect of Facing Inclination

The researchers carried out a numerical analysis to investigate the effect of the horizontal toe restraint on behavior of reinforced soil wall under working stress condition [46]. The effect of other factors on the wall behavior has been studied, including reinforced spacing, reinforcement stiffness, shear stiffness between blocks, the height of the wall, and wall facing inclination. Four types of the interface were considered in the numerical analysis: between backfill soil-reinforcement, backfill soil-foundation soil, block-block, backfill soil-wall facing, and the shear strength of the interface defined by the Mohr-Coulomb failure criterion. The value of wall-facing inclination (from vertical) adopted in parametric study was $\mathbf{0}°$, $\mathbf{4}°$, $\mathbf{8}°$, and $\mathbf{13}°$. The numerical result indicates that with the increase in the facing batter angle, the forces acting on the back of reinforced wall decreased. However, it has also been found that in some simulations, the load acting on the toe of the wall does not change, whereas the fraction of the total load carried by toe increase with the increase in the wall-facing batter angle (Fig. 13). Another study conducted the numerical analysis on the effect of geogrid layouts on behavior of GRS-RW in terms of failure mechanisms and displacement of the structure [47]. The same amount of geogrid was distributed by various layout, and effect of each layout on the behavior of reinforced soil structure was studied and compared. Three values of facing inclination (from horizontal) were adopted in numerical analysis, which are $\mathbf{70}°$, $\mathbf{80}°$, and $\mathbf{90}°$. The numerical result indicates that for the facing inclination of $\mathbf{70}°$ and $\mathbf{80}°$, the vertical settlement of the backfill surface was distributed uniformly except the area around slope crest (Fig. 14). This phenomenon indicates that the failure mechanisms of GRS-RW with a gentle wall-facing inclination is like a sliding mode. It was found that for GRS-RW with a facing inclination less than $\mathbf{80}°$, the horizontal displacement of the wall-facing is reduced significantly, and the deformation pattern is changed. Another study carried out a three-dimensional numerical study to investigate the effect of the friction angle between backfill soil and wall-facing, the backslope angle, and wall-facing inclination angle on the behavior of GRS-RW in terms of horizontal wall-facing displacements, maximum tensile loads within reinforcement layers, and potential failure surface under working stress conditions [48]. Four values of wall-facing inclination including $\mathbf{0}°$, $\mathbf{10}°$, $\mathbf{15}°$, and $\mathbf{20}°$ were adopted. The numerical result indicates that the facing inclination imposes impacts on critical slip surface and maximum tensile loads within reinforcement layers (Fig. 15). When wall-facing inclination is larger than $\mathbf{10}°$, the critical slip surface is shallower than the theoretical Rankine failure plane which agrees well with the AASHTO and FHWA design guidelines. In addition, the maximum reinforcement tensile loads decrease with the increase in the facing batter angle as the increase in earth pressure. The researchers carried out a finite element analysis combined with the probabilistic framework to investigate the effect of wall parameters such as wall height, soil properties, reinforcement spacing and stiffness, and the facing batter angle on wall behavior in terms of tensile strain within the reinforcement and maximum wall-facing displacement [49]. Three values of facing batter angle (from vertical) were adopted in numerical analysis: $\mathbf{0}°$, $\mathbf{5}°$, and $\mathbf{10}°$. The result from numerical analysis indicates that with the increase in facing batter angle (from vertical), the maximum horizontal displacement of wall-facing, the maximum connection strains, and the maximum tensile strains within reinforcement layers were all reduced. The decrease in these three factors was in good agreement with the earth pressure theory, which indicates that while other conditions are kept same, the forces acting on the reinforced soil wall decreases with the increase in wall-facing inclination. A previous study investigated the combined effect of uniformly distributed surcharge loads and wall-facing inclination on behavior of GRS-RW through experimental and numerical studies [50]. Three values of facing inclination were considered in the analysis: $\mathbf{6}°$, $\mathbf{15}°$, and $\mathbf{20}°$. The numerical result indicates that the large wall-facing inclination (to the vertical) reduces the tensile loads within the reinforcement. In AASHTO design guidelines of GRS-RW, the effects of uniform surcharge load and facing inclinations are considered independently. Moreover, only the determination of lateral earth pressure takes the facing inclination into account. For GRS-RW with small facing inclinations (to the vertical), the independent consideration of facing inclination may yield appropriate prediction in reinforcement tensile loads, and the difference of tensile loads between measurements and numerical predictions is little. However, with the increase in facing inclination to the large value, the discrepancies between measurements and numerical predictions appears and increases continuously. This phenomenon clearly indicates that the combined effect of surcharge load and facing inclinations needs to be considered for the prediction of tensile loads within the reinforcement layer. Table 1 provides the summarization of these aforementioned numerical analysis on the facing inclination of the GRS-RW.

**5.2 Effect of Reinforcement Length**

A previous study conducted a series of parametric studies on major design parameters of GRS-RW through a two-dimensional small-strain finite element analysis [51]. The investigated critical design parameters are soil properties of backfill soil and foundation soil, the interaction between facing blocks, and reinforcement stiffness, spacing, and the length. The relative importance of these major design parameters on tensile loads within reinforcement layers and wall-facing displacements is studied. A total of $\mathbf{48}$ analysis cases resulted from the variation of the investigated design parameters were conducted.

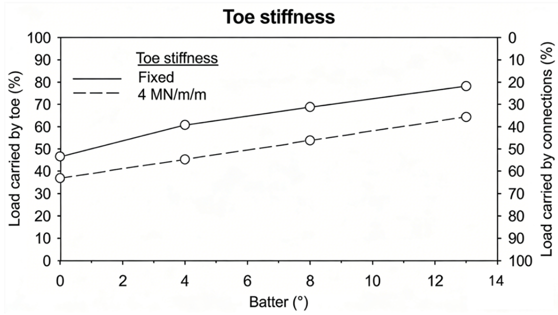


Fig. 13. Load carried by toe with the increase in facing batter [46]

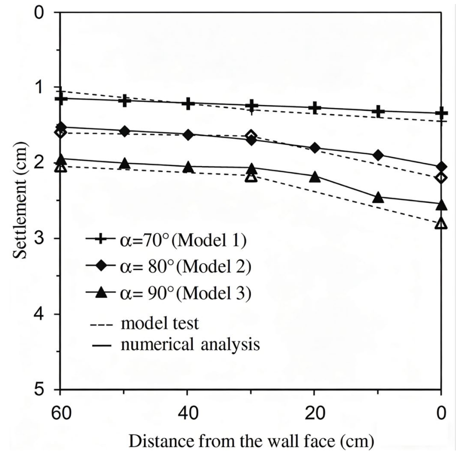


Fig. 14. Settlement at the top of the wall for various facing angles [47]

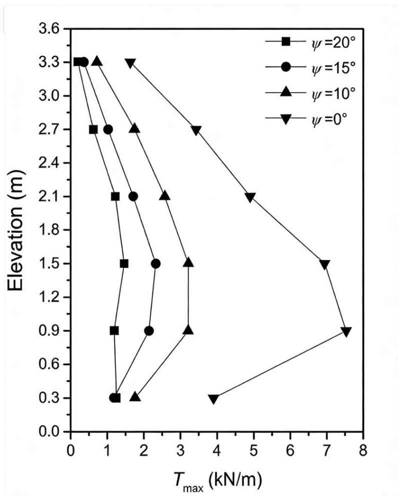


Fig. 15. Effect of facing batter angle on maximum reinforcement load [48]

Table 1. Summary of numerical studies of facing inclination effect

| No. | 1 | 2 | 3 | 4 | 5 |
|---|---|---|---|---|---|
| Authors | [46] | [47] | [48] | [49] | [50] |
| Numerical methods | FDM | FDM | FDM | FDM | FEM |
| Software | FLAC | FLAC | FLAC | FLAC | PLAXIS |
| 2D or 3D | 2D | 2D | 3D | 2D | 2D |
| H ($\boldsymbol{m}$) | $\mathbf{3.6}$-$\mathbf{12}$ | $\mathbf{0.8}$ | $\mathbf{3.6}$ | $\mathbf{4}$-$\mathbf{8}$ | $\mathbf{7.2}$ |
| L ($\boldsymbol{m}$) | $\mathbf{2.52}$-$\mathbf{8.4}$ | $\mathbf{0.375}$ | $\mathbf{2.22}$ | $\mathbf{2.8}$-$\mathbf{5.6}$ | $\mathbf{5}$ |
| S ($\boldsymbol{m}$) | $\mathbf{0.3}$-$\mathbf{0.9}$ | $\mathbf{0.1}$ | $\mathbf{0.6}$ | $\mathbf{0.6}$ | $\mathbf{0.4}$ |
| $\boldsymbol{\omega}$ (°) | $\mathbf{0}$-$\mathbf{13}$ (from vertical) | $\mathbf{70}$-$\mathbf{90}$ (from horizontal) | $\mathbf{0}$-$\mathbf{20}$ (from vertical) | $\mathbf{0}$-$\mathbf{10}$ (from vertical) | $\mathbf{6}$-$\mathbf{20}$ |
| Load on wall top | No load | Uniform vertical load | No load | Uniform vertical load | Uniform vertical load |
| BCM | Nonlinear elastic material with Duncan-Chang model | Nonlinear elastic stress-strain model with MC failure criterion | Elastic-perfectly plastic materials with MC failure criterion | Linear elastic model with MC failure criterion | Hyperbolic hardening soil model |
| RCM | Cable elements with linear load-strain properties | Elastic-plastic model with MC yield criterion | Linear elastic model | Cable elements | Linear elastic model |
| BRI | Linear spring-slider system with MC failure criterion | Cable elements | Linear spring-slider system with MC failure criterion | Soil-cable 'grout' interface | Perfectly bounded |
| BBI | Same as above | Cable elements | Same as above | Zero-thickness | No |
| BI | Same as above | No | Same as above | Same as above | No |
| CIS | Yes | No | Yes | Yes | Yes |
| Foundation type | Rigid | Compressible | Rigid | Rigid | Rigid |
| Stress conditions | Working stress | Ultimate strength | Working stress | Working stress | Working stress |

Note: MC: Mohr-Coulomb; FDM: finite difference method; FEM: finite element method; LA: limit analysis; H: height of wall; L: reinforcement length; S: spacing of reinforcement; CIS: compaction-induced stress; BI: blocks interface; BBI: block/backfill interface; BRI: backfill/reinforcement interface; RCM: reinforcement constitutive model; BCM: backfill soil constitutive model.

The numerical results indicate that considering the maximum displacements of the wall-facing and the tensile loads within reinforcement layers, the reinforcement length of $\mathbf{0.5}$ times the wall height can ensure the satisfactory behavior of the GRS-RW. Anther study carried out a numerical study to characterize the stability of the reinforced retaining wall by describing the effect of properties of backfill soil and foundation soil, reinforcement stiffness and length, and the surcharge load on the behavior of the reinforced retaining wall [52]. The numerical results indicated that the longer reinforcement layer requires less strength than the shorter reinforcement layer as some of the shorter reinforcement layers had little contribution because of the possibility of the pullout failure. Moreover, some layers of the short reinforcement may be within the active soil mass zone; the loss of the contribution to the overall stability from these reinforcement layers needs to be compensated by other reinforcement layers. Therefore, for the reinforcement layers with shorter length, the higher reinforcement strength is required. The researchers caried out a numerical study to investigate the failure mechanisms of the GRS-RW with extensible geogrid reinforcement layers through FEM [53] (Fig. 16). For the parametric study related to the length of reinforcement layer, the values were $\mathbf{0.5}$, $\mathbf{0.67}$, $\mathbf{1.0}$, and $\mathbf{1.5}$ times the wall height. The numerical result indicates that for reinforcement length equals $\mathbf{0.67}$, $\mathbf{1.0}$, and $\mathbf{1.5}$ times the wall height, the shear strain within the soil mass at the end of the construction is in good consistency with the locations of the maximum tensile load within reinforcement layer, which represents that the potential failure plane at the end of construction is within the reinforced soil zone. In addition, the overall safety factor significantly increases with the increase in reinforcement length. For GRS-RW under the critical limit state by the reduction in soil shear strength, there is a tendency that the reinforced soil zone is about to separate from the retained soil zone, and this tendency progressively disappears with the increase in the length of the reinforcement layer. Another study conducted a numerical investigation of the two-tier GRS-RW to determine the minimum length of reinforcement layers with respect to the offset distance [54]. Based on the numerical results, the minimum length of the reinforcement layer and the internal failure mechanisms were determined for GRS-RW with various offset distances. Adopting different values of reinforcement length and offset distances, several different analysis cases have been developed for the parametric study. The numerical result indicates that when the offset distance is larger than $\mathbf{0.7}$ times the height of the lower-tier, the critical slip surface will develop in the lower and upper tiers independently and approximately follow the shape of log-spiral. When the offset distance is lower than $\mathbf{2\,m}$, the minimum length of the reinforcement required is $\mathbf{1.25}$ times and the $\mathbf{0.9}$ times the respective tier height for the upper and lower tiers, respectively. When the offset distance is larger than $\mathbf{2\,m}$, the minimum length of the reinforcement layer required is $\mathbf{0.75}$ times and $\mathbf{0.7}$ times the respective tier height for the upper and the lower tiers, respectively. It is notable that the minimum length of the reinforcement for the lower tier is influenced more significantly than the upper tier by the distance of the offset, which indicates that the length of the reinforcement of the lower tier affects the stability of the wall to a larger extent than the upper tier (Fig. 17). A previous study employed a calibrated finite element procedure to study the deformation behavior of GRS-RW under working stress condition at the end of construction and in long-term [55]. The behavior of GRS-RW was studied for a $\mathbf{10}$-years creep under the effect of the gravity after the end of construction. Regarding each analysis case, the length of reinforcement layer ranges from $\mathbf{0.6}$ times to $\mathbf{1.2}$ times the wall height was adopted. The numerical result indicates that the reinforcement length imposes minor impact on the displacements of the reinforced soil zone, whereas the reinforced zone deformation is governed by the reinforcement stiffness and the spacing to a larger extent. In contrast, the horizontal deformation of the soil mass behind the reinforced soil zone is significantly influenced by the length of the reinforcement. Table 2 provides the summarization of these aforementioned numerical analysis on the length of geogrid layers.

### 5.3 Effect of Reinforcement Spacing

Another study investigated effect of spacing between geogrid reinforcement layers on failure mechanisms of GRS-RW through a parametric study [53]. Two values of reinforcement spacing were adopted, $\mathbf{0.5\,m}$ and $\mathbf{1.0\,m}$, respectively. The effect of reinforcement spacing was evaluated under two conditions, which are working condition and failure condition. The deformation of reinforced soil zone with close spacing of the reinforcement layer ($\mathbf{0.5\,m}$) is less than the model with large reinforcement layer spacing ($\mathbf{1.0\,m}$) under the failure condition.

It can be observed that for the model with $\mathbf{0.5\,m}$ reinforcement spacing, the reinforced soil zone still remains intact when the failure of wall initiates. For the model with the reinforcement spacing of $\mathbf{1.0\,m}$, the deformation of the soil mass is within the reinforced soil zone. It can be concluded that for the GRS-RW with close reinforcement spacing, the external failure modes are likely to occur. For the GRS-RW with large reinforcement spacing, the internal failure mode is possible to happen.

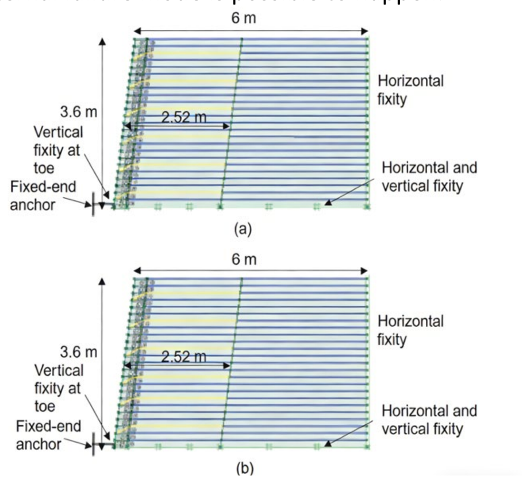


Fig. 16. Model components and geometry [53]

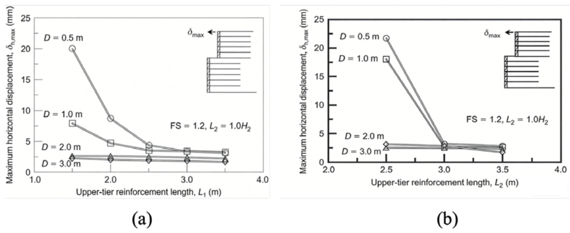


Fig. 17. (a) Effect of upper-tier reinforcement length; (b) Effect of lower-tier reinforcement length [54]

Table 2. Summary of numerical studies of the reinforcement length effect

| No. | 1 | 2 | 3 | 4 | 5 |
|---|---|---|---|---|---|
| Authors | [51] | [52] | [53] | [54] | [55] |
| Numerical methods | FEM | FDM | FEM | FEM | FEM |
| Software | M-CANDE | FLAC | PLAXIS | Abaqus | Swndyne |
| 2D or 3D | 2D | 2D | 2D | 2D | 2D |
| H ($m$) | $5.7$ | $9$ | $9$ | $5.5$ | $8.2$ |
| L ($m$) | $1.0$-$4.8$ | $4.2$-$6.3$ | $4.5$-$13.5$ | $1.5$-$3.5$ | $4.1$-$9.8$ |
| S ($m$) | $0.15$-$1.05$ | $0.6$ | $0.5$-$1.0$ | $0.2$-$0.6$ | $0.2$-$1.0$ |
| $\omega$ (°) | $0$ | $0$ | $0$ | $0$ | $0$ |
| Load on wall top | No load | Uniform vertical load | No load | No load | No load |
| BCM | Nonlinear elastic model | Perfectly elastoplastic model with MC failure criterion | Perfectly elastoplastic model with MC failure criterion | Elastoplastic model with MC failure criterion | Generalised plasticity model |
| RCM | Nonlinear elastic model | Cable elements | Tensile elastic model | Plasticity model with von Mises yield surface | Elastoplastic viscoplastic model |
| BRI | Fully-bounded | MC model | MC model | Fully-bounded | Perfectly bounding |
| BBI | Interface elements of stiffness method | MC model | Same as above | Defined by normal and tangential behaviour | MC model |
| BI | Same as above | Same as above | Same as above | Same as above | Same as above |
| CIS | No | No | No | No | Yes |
| Foundation type | Compressible | Compressible | Rigid | Rigid | Rigid |
| Stress conditions | Working stress | Working stress and ultimate strength | Working stress and ultimate strength | Working stress and ultimate strength | Working stress |

Note: MC: Mohr-Coulomb; FDM: finite difference method; FEM: finite element method; LA: limit analysis; H: height of wall; L: reinforcement length; S: spacing of reinforcement; CIS: compaction-induced stress; BI: blocks interface; BBI: block/backfill interface; BRI: backfill/reinforcement interface; RCM: reinforcement constitutive model; BCM: backfill soil constitutive model.

A previous study carried out a finite element numerical analysis considering the time-dependent reinforcement properties to investigate the reinforcement tensile load and its distribution within the structure in long-term period [56]. The effect of influencing factors such as the reinforcement stiffness, reinforcement length, reinforcement spacing, and properties of backfill soil on the long-term tensile load distribution within reinforcement layer was investigated. The numerical result indicates that the effect of spacing between reinforcement layers is more considerable than the effect of reinforcement length. With the increase in reinforcement spacing, the maximum tensile load within reinforcement layers increases (Fig. 18). It has also been found that the relationship between the maximum tensile load within reinforcement layers and the reinforcement spacing is almost linear at the end of the construction and after $10$ years of creep. In addition, the profile of the maximum tensile load within reinforcement layers was not only influenced by backfill soil shear strength, which was considered in most design methods, but was affected by reinforcement stiffness, reinforcement length, and reinforcement spacing. The researchers carried out a numerical study to optimize the reinforcement spacing of reinforcement layers through Limit Analysis, when the GRS-RW was subjected to the surcharge load [57]. The vertical spacing of reinforcement layers equals $0.2\ m$, which is defined as dense reinforcement spacing, and a ratio namely reinforcement density ratio (RDR) is defined as the ratio of the height of the wall with dense reinforcement spacing to the full height of wall. Five values of the RDR ratio have been adopted in the parametric study: 0.0, 0.25, 0.50, 0.75, and 1.0. The numerical results indicated that the effect of non-uniform reinforcement spacing is significantly influenced by the associated failure mechanism of the structure. The effect of placing the dense reinforcement within the wall gradually decreases with the increase in the strength of reinforcement, realizing that the uniform distribution of the reinforcement with 'normal' spacing may be more reasonable. However, the distribution of the reinforcement with the dense spacing and the low strength may be a more advantageous design. In addition, placing the dense reinforcements around the crest of the wall subjected to the surcharge load yields a significant improvement in the stability, while placing the dense reinforcement near the toe of the wall only improves the stability under self-weight condition. Another study carried out a finite element numerical analysis to study the effect of the design factors on the complex behavior of the GRS-RW subjected to spread footing [58]. A parametric study was conducted to investigate the effect of the design factors such as the reinforcement spacing, reinforcement type, footing dimensions, footing location, and the toe restraint on the distribution of reinforcement strains, the wall deformation, and the distribution of the lateral earth pressure within the structure. The numerical results indicated that the vertical spacing between layers of the reinforcement imposes significant impact of the behavior of GRS-RW subjected to spread footing under working stress state. With the decrease in the vertical spacing of reinforcement layers, the vertical settlement and lateral displacement of footings also decrease (Fig. 19). In addition, the earth pressure will be increased with the decrease in the reinforcement spacing. Lateral earth pressure not only depends on the reinforcement stiffness but the reinforcement spacing and the footing conditions. Using closer spacing of reinforcement or stiffer reinforcements may induce higher earth pressures, but the horizontal and vertical displacements of the wall can be reduced. A previous study carried out a nonlinear elastic method to investigate the tensile load within the reinforcement at the potential critical slip surface of GRS-RW without the restriction from wall-facing [59]. The numerical results indicated that Poisson's ratio significantly affects the soil volumetric deformation under vertical soil stress condition. If a constant Poisson's ratio is adopted to evaluate the tensile load of reinforcement, its value needs to be reasonably determined based on the mobilized soil strength in reinforced soil zone and the stress level. Moreover, using a constant value or varying values of Poisson's ratio to estimate the reinforcement loads is dependent on the reinforcement spacing and reinforcement stiffness. Table 3 provides the summarization of these aforementioned numerical analysis on the reinforcement spacing of the reinforced soil walls.

## 6. CONCLUSIONS

The geogrid-reinforced soil retaining wall has been used widely for slope stabilization and has been proved as a reliable approach against geological hazards. For a valid design of geogrid-reinforced soil retaining wall, it is necessary to have a deep insight into the typical failure mode of the geogrid-reinforced soil retaining wall. There are three types of the failure mode of geogrid-reinforced soil retaining wall, which are external instability, internal instability, and overall instability, respectively.

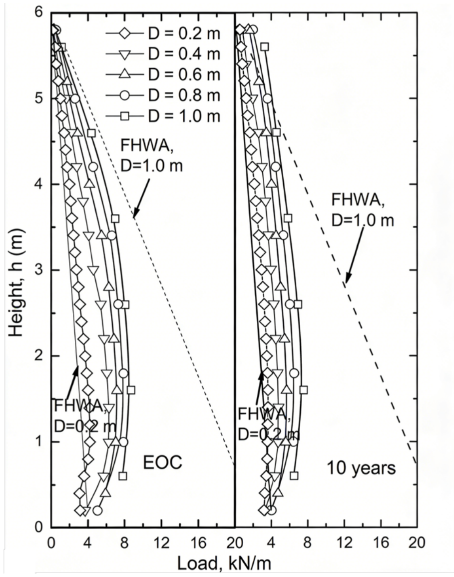


Fig. 18. Effect of reinforcement spacing on maximum reinforcement tensile load [56]

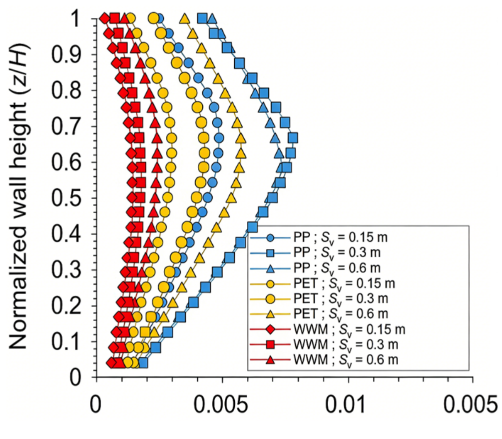


Fig. 19. Effect of vertical spacing on lateral displacement profile [58]

Table 3. Summary of numerical studies of the reinforcement spacing effect

| No. | 1 | 2 | 3 | 4 | 5 |
|---|---|---|---|---|---|
| Authors | [53] | [56] | [57] | [58] | [59] |
| Numerical methods | FEM | FEM | LA | FEM | Incremental method |
| Software | PLAXIS | Swandyne-Ⅱ | DLO-LA | Abaqus | Developed code |
| 2D or 3D | 2D | 2D | 2D | 2D | 2D |
| H ($m$) | 9 | 6 | 4.8 | 3.6 | 2-8 |
| L ($m$) | 4.5-13.5 | 3.0-5.0 | Full length | 2.22 | Full length |
| S ($m$) | 0.5-1.0 | 0.2-1.0 | 0.2-0.6 | 0.15-0.6 | 0.2-0.4 |
| $\omega$ (°) | 0 | 0 | 0 | 8 | 0 |
| Load on wall top | No load | No load | Strip footing | Strip footing | Uniform vertical load |
| BCM | Perfectly elastoplastic model with MC failure criterion | Generalised plasticity model | Elastoplastic model with MC failure criterion | Nonlinear elastic-plastic model | Hardening soil model |
| RCM | Tensile elastic model | Elastoplastic viscoplastic model | Tensile elastic model | Linear-elastic wire tensile elements | Nonlinear stress-strain model |
| BRI | MC model | Perfectly bounding | Planes for sliding or separation | Perfectly bounding | Nonlinear elastic models |
| BBI | Same as above | MC model | Same as above | Defined by normal and tangential behaviour | No |
| BI | Same as above | Same as above | Same as above | Same as above | Same as above |
| CIS | No | No | No | Yes | Yes |
| Foundation type | Rigid | Compressible | Rigid | Rigid | Rigid |
| Stress conditions | Working stress and ultimate strength | Working stress | Working stress | Working stress | Working stress |

Note: MC: Mohr-Coulomb; FDM: finite difference method; FEM: finite element method; LA: limit analysis; H: height of wall; L: reinforcement length; S: spacing of reinforcement; CIS: compaction-induced stress; BI: blocks interface; BBI: block/backfill interface; BRI: backfill/reinforcement interface; RCM: reinforcement constitutive model; BCM: backfill soil constitutive model.

The purpose of evaluating the external stability of geogrid-reinforced soil retaining wall is to determine the dimensional parameters of the reinforced soil section and guarantee is has sufficient size against the sliding, overturning at the toe, bearing capacity failure of the foundation soil, and the deep-seated instability. Regarding the internal instability evaluations, it can be adopted to determine the vertical spacing between layers of reinforcement, the length and the tensile strength of the geogrid reinforcement layers, as these factors will affect the pattern of the internal failure. Regarding the overall failure mechanism, constructing the geogrid-reinforced soil retaining wall on the slope will alter the stress field within the slope mass, potentially triggering the slope instability away from the range adjacent to the retaining wall. Moreover, it is worth noting that the overall failure pattern mainly depends on the properties of the soil and the reinforcement and the geometry of the slope.

After a comprehensive understanding of the failure mechanisms of geogrid-reinforced soil retaining wall, a wide variety of analysis methods have been developed and refined to study its effects on the stability of the embankment and slope. Regarding the Earth Pressure Theory, it has been used extensively to evaluate the tensile loads within the geogrid reinforcement layers based on the assumption that the lateral earth pressure in geogrid-reinforced soil retaining wall is in a state of equilibrium with the tensile forces generated in the geogrid reinforcement layers. In addition, the Limit

Equilibrium Method has also been extended to the design of geogrid-reinforced soil retaining wall. Regarding different analytical methods based on Limit Equilibrium Method, the assumption about the force inclination angle between vertical slices of the reinforced soil mass varies significantly. Compared with conventional Limit Equilibrium Method, several additional major assumptions will be introduced, including the distribution of the reinforcement tension along with the depth and the peak tensile forces within each geogrid reinforcement layer. Regarding the Finite Element Method, it has become an effective method to investigate the complicated behavior of geogrid-reinforced soil retaining wall, and also serve as a valuable complement to the traditional Limit Equilibrium Method due to its own advantages.

From a practical geotechnical perspective, the design parameters of the geogrid-reinforced soil retaining wall exert a critical impact on the behavior of embankment and slope. Regarding the wall-facing inclination, it has significant influence on the horizontal wall-facing displacements, maximum tensile loads generated in geogrid reinforcement layers, and the potential failure surface of the slope. In addition, the effect of wall-facing inclination on the stability of embankment and slope has also been discussed thoroughly. The geogrid reinforcement length also imposes significant impacts on the response of geogrid-reinforced soil retaining wall. The minimum recommended ratio of reinforcement length to the wall height is around $\mathbf{0.5}$ to ensure the satisfactory behavior of the geogrid-reinforced soil retaining wall. Moreover, the length of the geogrid reinforcement layer has a significant impact on the failure mechanism of the geogrid-reinforced soil retaining wall. Regarding the vertical spacing between geogrid reinforcement layers, the recommended value is various. It has been found that with the decrease in the reinforcement spacing, the effect of restraining considerably increases. In addition, placing the dense reinforcements around the crest of the slope may yield a significant improvement in the slope stability.

In general, this study has presented a comprehensive review on the geogrid-reinforced soil retaining wall in terms of different failure modes, analysis methodology, and the determination of critical design parameters. Recent developments in Finite Element Method and the extension in traditional Limit Equilibrium Method for the purpose of investigating the behavior of geogrid-reinforced soil retaining wall has also been reviewed. The determination of the critical design parameters which relates to the behavior of the geogrid-reinforced soil retaining wall have also been discussed and summarized thoroughly. Regarding the study related to the geogrid-reinforced soil retaining wall in the future, the interaction between the geogrid reinforcement layer and the backfill soil needs to be studied further. In addition, more emphasis can be placed on the innovation of new geogrid materials and the dynamic response characteristics of the geogrid-reinforced soil retaining wall.

## 7. REFERENCES


1. Xu P., Hatami K., Bao J. and Li T. Bearing capacity and failure mechanisms of two-tiered reinforced soil retaining walls under footing load. Computers and Geotechnics 128 2020, pp.103833. https://doi.org/10.1016/j.compgeo.2020.103833
2. Yang G., Zhang B., Lv P. and Zhou Q. Behaviour of geogrid reinforced soil retaining wall with concrete-rigid facing. Geotextiles and Geomembranes 27(5) 2009, pp.350-356. https://doi.org/10.1016/j.geotexmem.2009.03.001
3. Yu Y., Bathurst R.J., Allen T.M. and Nelson R. Physical and numerical modelling of a geogrid-reinforced incremental concrete panel retaining wall. Canadian Geotechnical Journal 53(12) 2016, pp.1883-1901. https://doi.org/10.1139/cgj-2016-0207
4. Wang Y., Smith J.V. and Nazem M. Optimization of a slope-stabilization system combining gabion-faced geogrid-reinforced retaining wall with embedded piles. KSCE Journal of Civil Engineering 25(12) 2021, pp.4535-4551. https://doi.org/10.1007/s12205-021-1300-6
5. Zhu Y, Zhan Z, Hong Y, Guo P, He M, Chen R. Experimental study on mechanical and deformation characteristics of geogrid-reinforced soil retaining walls. International Journal of Geosynthetics and Ground Engineering 10(5) 2024, pp.74. https://doi.org/10.1007/s40891-024-00585-9
6. Tulebekova A, Kusbergenova Z, Dosmukhambetova B, Bakirova D, Tleulenova G, Zhumadilov I. Effects of geogrid and non-woven geotextiles on the shear behavior of soil. GEOMATE Journal 27(123) 2024, pp.75-82. https://doi.org/10.21660/2024.123.4633
7. Abdoli Fazel A., Fahimifar A., Emami Tabrizi M. and Nazari Afshar J. Numerical Analysis of Back-to-Back Geogrid-Reinforced Modular-Block Walls Under Service Stresses: Interaction Behavior and Design Insights. Geotechnical and Geological Engineering 43(2) 2025, pp.97.

https://doi.org/10.1007/s10706-024-03064-0
8. Hoang DP. 2D Analyses of Global Stability of a Geosynthetic-Reinforced Mechanically Stabilized Earth Retaining Wall with Different Soil Conditions. GEOMATE Journal 29(135) 2025, pp.146-54. https://doi.org/10.21660/2025.135.5177
9. Wang Y. Comparison of Concrete-Rigid Facing and Gabion Basket-Flexible Facing of Geogrid-Reinforced Soil Retaining Walls Subject to Various Loading Conditions. Indian Geotechnical Journal 27 2025, pp.1-7. https://doi.org/10.1007/s40098-025-01458-2
10. Elias V., Christopher B.R., Berg R.R. and Ryan R.B. Mechanically stabilized earth walls and reinforced soil slopes: design and construction guidelines (updated version) (No. FHWA-NHI-00-043). United States. Federal Highway Administration 2001.
11. Christopher B.R., Leshchinsky D. and Stulgis R. 2005. Geosynthetic-reinforced soil walls and slopes: US perspective. International Perspectives on Soil Reinforcement Applications, pp.1-12. https://doi.org/10.1061/40788(167)12
12. Leshchinsky D., Leshchinsky O., Zelenko B. and Horne J. Limit equilibrium design framework for MSE structures with extensible reinforcement (No. FHWA-HIF-17-004). United States. Federal Highway Administration. Office of Bridge Technology, 2016.
13. Song F., Liu H., Ma L. and Hu H. Numerical analysis of geocell-reinforced retaining wall failure modes. Geotextiles and geomembranes 46(3) 2018, pp.284-296. https://doi.org/10.1016/j.geotexmem.2018.01.004
14. Zhang B., Song F. and Liu J. Development and application of a nonlinear stress dilatancy model for geocell-reinforced soil via the FEM. Geotextiles and Geomembranes 53(4) 2025, pp.999-1020. https://doi.org/10.1016/j.geotexmem.2025.03.010
15. Schlosser F., 1990. Mechanically stabilized earth retaining structures in Europe, Design and Performance of Earth Retaining Structures. Geotechnical Special Publication (25) 1990, pp.347-378.
16. Leshchinsky D., Ling H. and Hanks G. 1995. Unified design approach to geosynthetic reinforced slopes and segmental walls. Geosynthetics International 2(5) 1995, pp.845-881. https://doi.org/10.1680/gein.2.0039
17. Rowe R.K. and Skinner G.D. Numerical analysis of geosynthetic reinforced retaining wall constructed on a layered soil foundation. Geotextiles and geomembranes 19(7) 2001, pp.387-412. https://doi.org/10.1016/S0266-1144(01)00014-0
18. Hatami K. and Bathurst R.J. 2005. Development and verification of a numerical model for the analysis of geosynthetic-reinforced soil segmental walls under working stress conditions. Canadian Geotechnical Journal 42(4) 2005, pp.1066-1085. https://doi.org/10.1139/t05-040
19. Linhares R.M., Mirmoradi S.H. and Ehrlich M. 2021. Evaluation of the effect of surcharge on the behavior of geosynthetic-reinforced soil walls. Transportation Geotechnics 31 2021, pp.100634. https://doi.org/10.1016/j.trgeo.2021.100634
20. Bishop AW. The use of the slice circle in the stability of slopes. Geotechnique, 1955.
21. Janbu N. Stability analysis of slopes with dimensionless parameters, Harvard University, Division of Engineering and Applied Physics, 1959.
22. Morgenstern N.U. and Price V.E. The analysis of the stability of general slip surfaces. Geotechnique 15(1) 1965, pp.79-93. https://doi.org/10.1680/geot.1965.15.1.79
23. Spencer E. (1967). A method of analysis of the stability of embankments assuming parallel inter-slice forces. Geotechnique 17(1) 1967, pp.11-26. https://doi.org/10.1680/geot.1967.17.1.11
24. Abdelmawla AM. Characterization of Geogrid Pullout Mechanism for Calcareous Sand Backfill. Master's Thesis, Cairo University Giza, Cairo, Egypt, 2017.
25. Ortigao J.A.R. Handbook of slope stabilisation, Springer Science & Business Media, 2004.
26. Duncan J.M., Wright S.G. and Brandon T.L. Soil strength and slope stability, John Wiley & Sons, 2014.
27. Murray R. 1981. Fabric reinforced earth walls: development of design equations, 1981, pp.0266-7045.
28. Collin J.G. Earth Wall Design (Reinforcement, Soil-Structure, Finite-Element Analysis), thesis, University of California, Berkeley, 1986.
29. Bonaparte R., Holtz R.D. and Giroud J. Soil reinforcement design using geotextiles and geogrids. Geotextile testing and the design engineer, ASTM International, 1987.
30. Simac M., Christopher B. and Bonczkiewicz C. 1990. Instrumented field performance of a 6 m geogrid soil wall. Proceedings of 4th Int.

Conference on Geotextiles, Geomembranes, and Related Products, 53-59.
31. Leshchinsky D. and Perry E.B. On the design of geosynthetic-reinforced walls. Geotextiles and geomembranes 8(4) 1989, pp.311-323. https://doi.org/10.1016/0266-1144(89)90014-9
32. Bathurst RJ. and Simac MR, 1994. Geosynthetic reinforced segmental retaining wall structures in North America. Proceedings of Fifth International Conference on Geotexiles, Geomembranes, and Related Products, 1-41.
33. Hammouri N.A., Malkawi A.I.H. and Yamin M.M. Stability analysis of slopes using the finite element method and limiting equilibrium approach. Bulletin of Engineering Geology and the Environment 67(4) 2008, pp.471-478. https://doi.org/10.1007/s10064-008-0156-z
34. Tan D. and Sarma S. Finite element verification of an enhanced limit equilibrium method for slope analysis. Geotechnique 58(6) 2008, pp.481-487. https://doi.org/10.1680/geot.2008.58.6.481
35. Seed, R., Collin, J. and Mitchell, J. 1986. FEM analyses of compacted reinforced soil walls. International symposium on numerical models in geomechanics, 553-562.
36. Ho S.K. and Rowe R.K. 1994. Predicted behavior of two centrifugal model soil walls. Journal of geotechnical engineering 120(10) 1994, pp.1845-1873. https://doi.org/10.1061/(ASCE)0733-9410(1994)120:10(1845)
37. Dashti F., Dhakal R.P. and Pampanin S. A parametric study on out-of-plane instability of doubly reinforced structural walls. Part I: FEM predictions. Bulletin of Earthquake Engineering 18(8) 2020, pp.3747-3780. https://doi.org/10.1007/s10518-020-00828-w
38. Skinner G.D. and Rowe R.K. Design and behaviour of a geosynthetic reinforced retaining wall and bridge abutment on a yielding foundation. Geotextiles and geomembranes 23(3) 2005, pp.234-260. https://doi.org/10.1016/j.geotexmem.2004.10.001
39. Hatami K. and Bathurst R.J. (2006) Numerical model for reinforced soil segmental walls under surcharge loading. Journal of Geotechnical and Geoenvironmental engineering 132(6) 2006, pp.673-684. https://doi.org/10.1061/(ASCE)1090-0241(2006)132:6(673)
40. Yoo C. and Kim S.B. Performance of a two-tier geosynthetic reinforced segmental retaining wall under a surcharge load: Full-scale load test and 3D finite element analysis. Geotextiles and geomembranes 26(6) 2008, pp.460-472. https://doi.org/10.1016/j.geotexmem.2008.05.008
41. Huang B., Bathurst R.J. and Hatami K. Numerical study of reinforced soil segmental walls using three different constitutive soil models. Journal of Geotechnical and Geoenvironmental engineering 135(10) 2009, pp.1486-1498. https://doi.org/10.1061/(ASCE)GT.1943-5606.0000092
42. Abdelouhab A., Dias D. and Freitag N. Numerical analysis of the behaviour of mechanically stabilized earth walls reinforced with different types of strips. Geotextiles and geomembranes 19(2) (2011), pp.116-129. https://doi.org/10.1016/j.geotexmem.2010.10.011
43. Mehdipour I., Ghazavi M. and Moayed R.Z. Numerical study on stability analysis of geocell reinforced slopes by considering the bending effect. Geotextiles and geomembranes 37 2013, pp.23-34. https://doi.org/10.1016/j.geotexmem.2013.01.001
44. Yu Y., Damians I.P. and Bathurst R.J. Influence of choice of FLAC and PLAXIS interface models on reinforced soil–structure interactions. Computers and Geotechnics 65 2015, pp164-174. https://doi.org/10.1016/j.compgeo.2014.12.009
45. Yu Y., Bathurst R.J. and Allen T.M. Numerical modelling of two full-scale reinforced soil wrapped-face walls. Geotextiles and geomembranes 45(4) 2017, pp.237-249. https://doi.org/10.1016/j.geotexmem.2017.02.004
46. Huang B., Bathurst R.J., Hatami K. and Allen T.M. Influence of toe restraint on reinforced soil segmental walls. Canadian Geotechnical Journal 47(8) 2010, pp.885-904. https://doi.org/10.1139/T10-002
47. Chen R.H., Wu C.P., Huang F.C. and Shen C.W. Numerical analysis of geocell-reinforced retaining structures. Geotextiles and geomembranes 39 2013, pp.51-62. https://doi.org/10.1016/j.geotexmem.2013.07.003
48. Rahmouni O., Mabrouki A., Benmeddour D. and Mellas M. A numerical investigation into the behavior of geosynthetic-reinforced soil segmental retaining walls. International Journal of Geotechnical Engineering 10(5) 2016, pp.435-444. https://doi.org/10.1080/19386362.2016.1158443

49. Yu Y. and Bathurst R.J. Probabilistic assessment of reinforced soil wall performance using response surface method. Geosynthetics International 24(5) 2017, pp.524-542. https://doi.org/10.1680/jgein.17.00019
50. Mirmoradi S., Ehrlich M., Chinchay P. and Dieguez C. (2019). Evaluation of the combined effect of facing inclination and uniform surcharge on GRS walls. Geotextiles and geomembranes 47(5) 2019, pp.685-691. https://doi.org/10.1016/j.geotexmem.2019.10 3485
51. Ling H. and Leshchinsky D. (2003). Finite element parametric study of the behavior of segmental block reinforced-soil retaining walls. Geosynthetics International 10(3) 2003, pp.77-94. https://doi.org/10.1680/gein.2003.10.3.77
52. Leshchinsky D. and Han J. (2004). Geosynthetic reinforced multitiered walls. Journal of Geotechnical and Geoenvironmental engineering 130(12) 2004, pp.1225-1235. https://doi.org/10.1061/(ASCE)1090-0241(2004)130:12(1225)
53. Guler E., Hamderi M. and Demirkan M. Numerical analysis of reinforced soil-retaining wall structures with cohesive and granular backfills. Geosynthetics International 14(6) 2007, pp.330-345. https://doi.org/10.1680/gein.2007.14.6.330
54. Yoo C., Jang Y. and Park I. Internal stability of geosynthetic-reinforced soil walls in tiered configuration. Geosynthetics International 18(2) 2011, pp.74-83. https://doi.org/10.1680/gein.2011.18.2.74
55. Liu H. Long-term lateral displacement of geosynthetic-reinforced soil segmental retaining walls. Geotextiles and geomembranes 32 2012, pp.18-27. https://doi.org/10.1016/j.geotexmem.2011.12.001
56. Liu H. and Won M.S. Long-term reinforcement load of geosynthetic-reinforced soil retaining walls. Journal of Geotechnical and Geoenvironmental engineering 135(7) 2009, pp.875-889. https://doi.org/10.1061/(ASCE)GT.1943-5606.0000052
57. Xie Y. and Leshchinsky B. MSE walls as bridge abutments: Optimal reinforcement density. Geotextiles and geomembranes 43(2) 2015, pp.128-138. https://doi.org/10.1016/j.geotexmem.2015.01.002
58. Ambauen S., Leshchinsky B., Xie Y. and Rayamajhi D. Service-state behavior of reinforced soil walls supporting spread footings: a parametric study using finite-element analysis. Geosynthetics International 23(3) 2016, pp.156-170. https://doi.org/10.1680/jgein.15.00039
59. Liu H. Nonlinear elastic analysis of reinforcement loads for vertical reinforced soil composites without facing restriction. Journal of Geotechnical and Geoenvironmental engineering 142(6) 2016, pp.04016013. https://doi.org/10.1061/(ASCE)GT.1943-5606.0001464